Boundary-Layer Meteorology (2026) 192:21
https://doi.org/10.1007/s10546-026-00963-y

REVIEW ARTICLE

# The Natural Laboratory of the Solar Eclipse for Investigating Switching of Surface Layer Turbulent Fluxes

**Thomas Foken**[1] · **R. Giles Harrison**[2]

Received: 19 August 2025 / Accepted: 6 February 2026


**Abstract**
Solar eclipses are astronomical phenomena generating multiple influences on atmospheric processes, with short-wave radiation effects having been studied extensively. In contrast, there are relatively few studies on turbulent fluxes. This paper reviews effects of total solar eclipses on turbulent fluxes at the Earth's surface, the local wind conditions, and time delays in the associated responses. Such investigations effectively occur within an unusual natural laboratory, providing the responses of atmospheric phenomena under predictable and rapidly changing radiative forcing, similar to that occurring during convective cloud cover changes. Recommendations are provided on how to optimise investigations to exploit the unique circumstances presented by future total solar eclipses, including through utilising the several hundred suitable measuring stations worldwide already operating continuously within existing research programmes.

**Keywords** Afternoon transition · Solar eclipse · Surface layer · Turbulent fluxes · Wind field

## 1 Introduction

Solar eclipses are not just an astronomical spectacle that attract interested observers. They have also fascinated meteorologists for almost 200 years, with the first quantitative studies of atmospheric changes made in the mid-1830s (e.g., Anonymous 1834; Birt 1836; Jenyns 1858), as reliable meteorological measurement technology became increasingly available, as demonstrated in the historical chapters by Foken (2021). Until the middle of the twentieth century, investigations focused on simple and clearly observed dependences, such as those between solar radiation and air temperature. Following this initial phase, a wider range of phenomena were investigated, spanning processes from the surface to the ionosphere. Comprehensive summaries of previous observations are contained within meteorological publications elsewhere, primarily concerning total solar eclipses (Aplin et al. 2016; Elmhamdi et al. 2024).

✉ R. Giles Harrison
r.g.harrison@reading.ac.uk

[1] Bayreuth Center of Ecology and Environmental Science, University of Bayreuth, 95440 Bayreuth, Germany

[2] Department of Meteorology, University of Reading, Reading RG6 6ET, UK

Published online: 10 March 2026

This paper seeks to review eclipse-influenced processes in the atmospheric boundary layer, with a focus on the measurement of turbulent fluxes near the surface. Table 1 gives an overview of many of the existing publications, mostly from research occurring in the last 50 years.

The fundamental utility of the eclipse arises from the precisely determined modulation of the extraterrestrial irradiance. This allows the response of various variables and processes to be studied. A solar eclipse can effectively be regarded as a 'natural laboratory experiment' with rapid onset and cessation, suitable for investigating processes within a temporally changing, but predictable, radiation environment. The value of this unique research opportunity for meteorology in general has been highlighted from previous investigations (Anderson 1999; Foken et al. 2001; Harrison and Hanna 2016).

The aim of this article is to highlight the processes that can be studied in the 'natural solar eclipse laboratory', with an emphasis on fluxes and their interaction with boundary layer processes, in turn closely linked to processes in the biosphere through heat and water vapor transport.

## 2 Problem and Measurement Possibilities

Figure 1 illustrates the typical sequence of changes during a total solar eclipse at a given location, and the response occurring in the meteorological elements as the zone of totality moves across the Earth's surface. Before totality, the air and the Earth's surface remain relatively warm even though the solar radiation may have already decreased significantly, but the phase of considerable cooling begins from the moment of totality. This creates a large spatial temperature gradient and, as a result, a pressure gradient. In turn, this causes strong winds before or during totality. After totality, it takes a long time for the air and the Earth's surface to warm again. During this phase of the eclipse, the temperature and pressure gradients are only slight, with an associated decrease in wind speed.

Three main areas of meteorological investigation can be identified for this typical set of circumstances:

- *Reaction times of meteorological elements and biophysical variables* to the radiative forcing, such as the reaction of photosynthesis to changing radiation
- *Dependence of meteorological elements on wind speed and radiative forcing*, such as atmospheric stability during the passage of an isolated cumulus cloud
- *Change in meteorological elements with decreasing or increasing radiation*, such as during the daily afternoon or morning transition.

A prerequisite for such investigations is that these dependencies can be measured at a greater rate than the changes which occur. The duration of totality is usually only 2 to 5 min. This means that measuring instruments with time constants less than 15–30 s are required for adequate temporal sampling. This is generally the case for wind and radiation measurements, but for accurate temperature and humidity measurements, only sensitive ventilated devices are fully suitable (Foken and Bange 2021). However, measuring the sensible and latent heat flux and the gas fluxes using the eddy covariance method is problematic. Although sonic anemometers and gas analysers easily meet the required time responses, the overall method itself requires averaging times of up to 30 min, and even longer with stable stratification. Figure 2 shows the $CO_2$ flux with moving average in the foreground of 30 min and in the background of 5 min. The 30-min averaging shows the respiration (positive $CO_2$ flux) during the totality, but with a blurred temporal resolution. Shortening the time interval provides

**Table 1** Total Solar eclipse related experimentation with boundary layer investigations

| Date | Time (UTC) | Eclipse type (if not total) | Region | References |
|---|---|---|---|---|
| October 23, 1976 | 0512:59 | | Australia | Antonia et al. (1979) |
| February 16, 1980 | 0854:01 | | India | Aplin et al. (2016), Kapoor et al. (1982) |
| July 11, 1991 | 1907:01 | Partial | USA | Mauder et al. (2007) |
| May, 10, 1994 | 1712:27 | Partial (94%) | New Mexico USA | Eaton et al. (1997) |
| February 26, 1998 | 1729:27 | | Venezuela | Peñazola-Murillo (2002) |
| August 11, 1999 | 1104:09 | | Europe | Aplin and Harrison (2003), Foken et al. (2001), Harrison and Gray (2017), Jenki et al. (1999), Leeds-Harrison et al. (2002), Provod (2010) |
| November 23, 2003 | 2250:22 | | Antarctica | Kameda et al. (2009) |
| March 29, 2006 | 1012:23 | | Greece (partial), Nigeria | Economou et al. (2008), Founda et al. (2007), Nymphas et al. (2012) |
| August 01, 2008 | 1012:12 | Partial (93%) | Svalbard | Sjöblom (2010) |
| March 20, 2015 | 0946:47 | | UK, Svalbard | Harrison and Gray (2017), Harrison and Hanna (2016), Schulz et al. (2017), Maturilli and Ritter (2016) |
| March 09, 2016 | 0158:19 | | Indonesian | Satyaningsih et al. (2016) |
| August 21, 2017 | 1826:40 | | USA | Fowler et al. (2019), Hicks et al. (2021), Higgins et al. (2019), |
| July 02, 2019 | 1926:08 | | Chile | Lazzus et al. (2022) |
| December 26, 2019 | 0518:53 | Annular | Saudi Arab | Elmhamdi et al. (2024), Madhavan and Venkat Ratnam (2021) |
| June 21,2020 | 0641:15 | Annular | Saudi Arab | Elmhamdi et al. (2024) |
| December 4, 2021 | 0734:38 | | Antarctica | Garreaud et al. (2023) |

**Table 1** (continued)

| Date | Time (UTC) | Eclipse type (if not total) | Region | References |
|---|---|---|---|---|
| April 08, 2024 | 1818:29 | | USA | Wang et al. (2024) |
| March 29, 2025 | 1048:36 | Partial | Europa, USA | this paper |

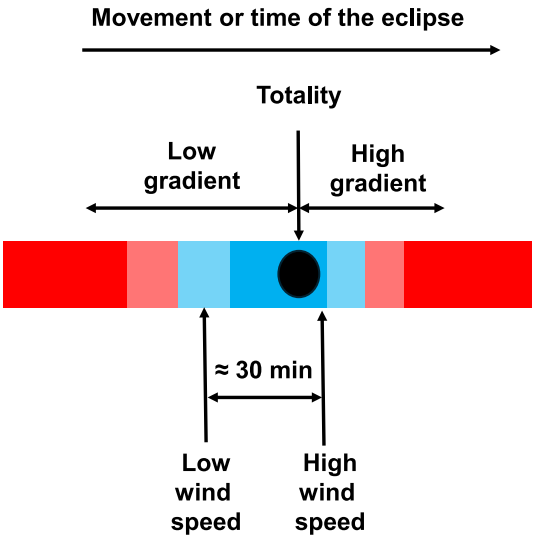


**Fig. 1** Schematic illustration of the temperature and wind (and their rates of change) during the passage through the totality zone of the solar eclipse. The colour scale (blue to red denoting cold to hot) qualitatively indicates the change in temperature

increased detail in temporal resolution, but energy components in the low-frequency range are not detected, so that the total flux is underestimated.

The detailed approach employed for these and related calculations is relevant to the comparisons which can be made from the quantities derived. A formal description for determining the flow can be given by integration across wavelet coefficients (Hudgins et al. 1993; Torrence and Compo 1998; Percival and Walden 2000) as:

$$\overline{x'y'} = \frac{\delta_t}{C_\delta} \cdot \frac{\delta_j}{N} \cdot \sum_{n=0}^{N-1} \sum_{j=0}^{J} \frac{\left[T_x(a,b) \cdot T_y^*(a,b)\right]}{a(j)}. \tag{1}$$

In this expression, $x(t)$ and $y(t)$ are the two simultaneously recorded time series which are being combined, $N$ is a given number of values in the time series during a time step $\delta_t$. $C_\delta$ is a wavelet-specific reconstruction factor, with $\delta_j$ referring to the spacing between discrete scales. $J$ is the maximum number of scales, $T_x(a,b)$ is the wavelet transform of the first time series $x(t)$, and $T_y^*(a,b)$ is the complex conjugate of the wavelet transform of the second time series $y(t)$.

A practical application of this approach which provided a comparison with other methods was described by Schaller et al. (2017), and is shown in Sect. 3.1, for the total solar eclipse on 20 March 2015 (Schulz et al. 2017). The original data were obtained at 10 to 20 Hz resolution. In general, standard correction procedures such as coordinate rotation, the correction of

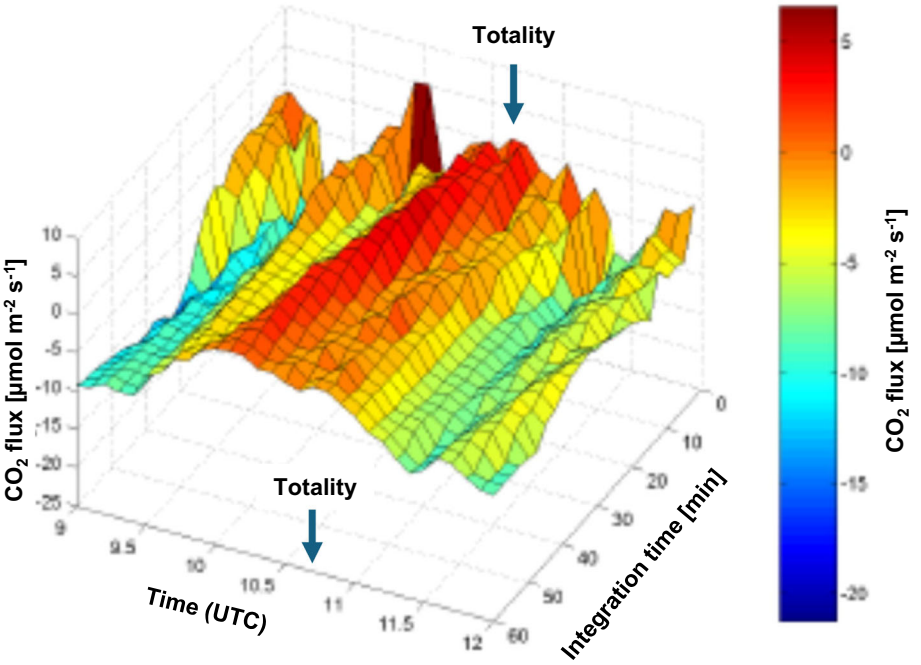


**Fig. 2** Determination of $CO_2$–flux during the total solar eclipse on 11 August 1999 (totality 1038.5 UTC, Freising, Germany) with different moving integration times from 30 min (front) to 5 min (rear) according to Foken et al. (2000), graph B. Wichura, © Authors

spectral losses, and other relevant corrections are required if quantitative results are desired for comparison purposes. For qualitative results, the correction for coordinate rotation is a minimum requirement, preferably using a planar fit over the investigation period of several hours (Foken et al. 2012; Mauder et al. 2021).

## 3 Main Areas of Investigation

In line with the three main research opportunities outlined in Sec. 2 of response times, prescribed forcing and local changes, some selected results of previous investigations are now presented and discussed.

### 3.1 Response Time of Different Fluxes and Variables

The time lag between the moment of totality and the minimum air temperature has been studied for many eclipses, with Anderson (1999) providing a good overview. However, in some cases, the time constant of the sensors used was greater than that ideally required, and/or the averaging interval was too long to provide an accurate representation of the micrometeorological changes. Therefore, the following discussion is based on measurements in which variables were measured at approximately 1-min intervals. Table 2 shows the time difference between the maximum totality and the reaction of various fluxes or variables. It is obvious

**Table 2** Lag time between maximum totality and reaction of fluxes and variables

| Variable | Lag time (minutes) | References |
|---|---|---|
| Air temperature (2 m) | 15 ± 3 | Foken et al. (2001), Founda et al. (2007), Satyaningsih et al. (2016), Fowler et al. (2019), Elmhamdi et al. (2024), Wang et al. (2024) |
| Air temperature (2 m), low angle of the sun | 30 | Kameda et al. (2009), Garreaud et al. (2023) |
| Wind speed | 24 ± 7 | Sjöblom (2010), Nymphas et al. (2012), Schulz et al. (2017'), Fowler et al. (2019), Higgins et al. (2019), Wang et al. (2024) |
| Sensible heat flux | 2 ± 2 | Foken et al. (2001), Schulz et al. (2017), Higgins et al. (2019), |
| Latent heat flux | 25 | Foken et al. (2001) |
| Friction velocity | 20 ± 5 | Foken et al. (2001), Schulz et al. (2017), |
| $CO_2$ flux | < 5 | Foken et al. (2001) |

that fluxes strongly linked to solar radiation, such as sensible heat flux and plant physiological fluxes, react very quickly. The same applies to the air temperature with some delay, and also to the temperature in bare soil (Leeds-Harrison et al. 2002). There is also a clear dependence on the solar elevation after the totality phase, Kameda et al. (2009), as the data from Antarctica show. In contrast, the friction velocity, and thus also the atmospheric stability, react more slowly (see also Fig. 1). However, it should be noted that the latent heat flux reacts significantly slower than the sensible heat flux.

The $CO_2$ flux was shown in Fig. 2 as an example of the response of physiologically generated fluxes. A similar figure was given by Hicks et al. (2021). Direct measurements of photosynthesis were carried out by Economou et al. (2008) and Foken et al. (2000), which are shown in Fig. 3.

The behaviour of the sensible heat flux and friction velocity at 1-min resolution using Eq. (1) is shown in Fig. 4. The friction velocity follows the wind speed and is small at about 30 min after the eclipse. The sensible heat flux is near zero under Arctic Spring conditions at – 20 °C, but briefly becomes strongly negative during totality. However, the reduced friction velocity has the strongest influence on stability, see Sect. 3.3.

### 3.2 Behaviour of the Wind Speed

The conceptual picture of Fig. 1 showed an increase in wind speed before the onset of totality and a decrease in wind speed having a minimum approximately 30 min after totality. This reduction during the half-hour after totality is also reflected in measurements, as shown in Fig. 5. The wind speed reduction is usually accompanied by a slight shift in wind direction. Table 3 contains a summary of the available results.

The changes in the wind field also impact mesoscale circulations although no fully comprehensive studies are available. A conceptual model for an 'Eclipse Cyclone' was developed by Clayton (1901a, b) based on measurements taken during the total solar eclipse on 28 May

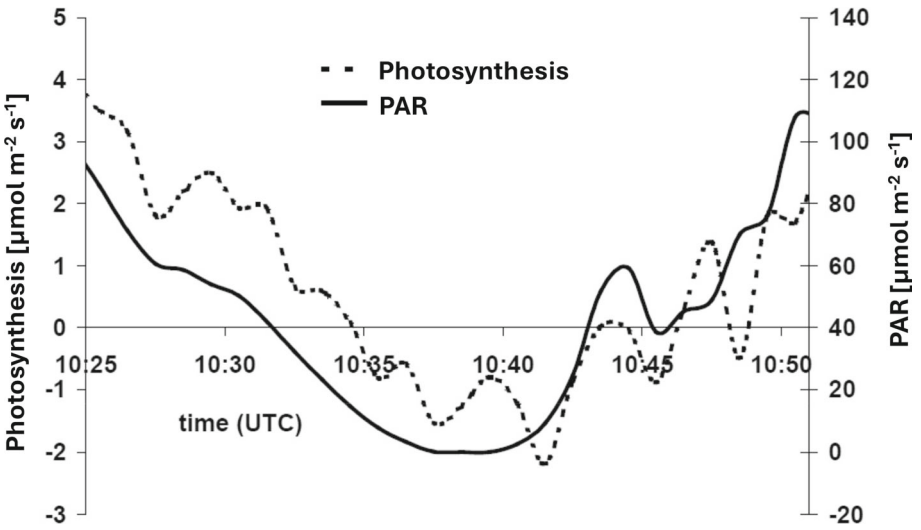


**Fig. 3** Dependence of photosynthesis (left axis) of a corn field measured with several LI-6400P (LI-COR, Lincoln, Nebraska, USA) devices on photosynthetically active radiation (PAR), (right axis), measured during the total solar eclipse on 11 August 1999 in Freising (Germany) according to Foken et al. (2000), graph from T. Kartschall, © Authors

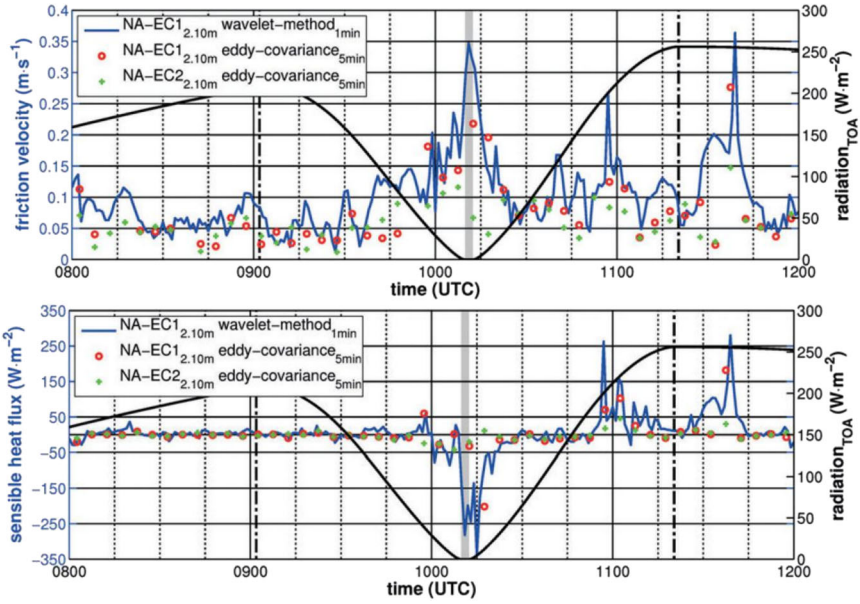


**Fig. 4** High-resolution measurements of friction velocity and sensible heat flux during the total solar eclipse on 20 March 2015 in Ny-Ålesund, Svalbard, according to Schulz et al. (2017), The wavelet analysis is shown with a resolution of 1 min. Furthermore, a 5-min classic analysis is shown for two measurement complexes, which is restricted in its coverage of the frequencies concerned, © Authors

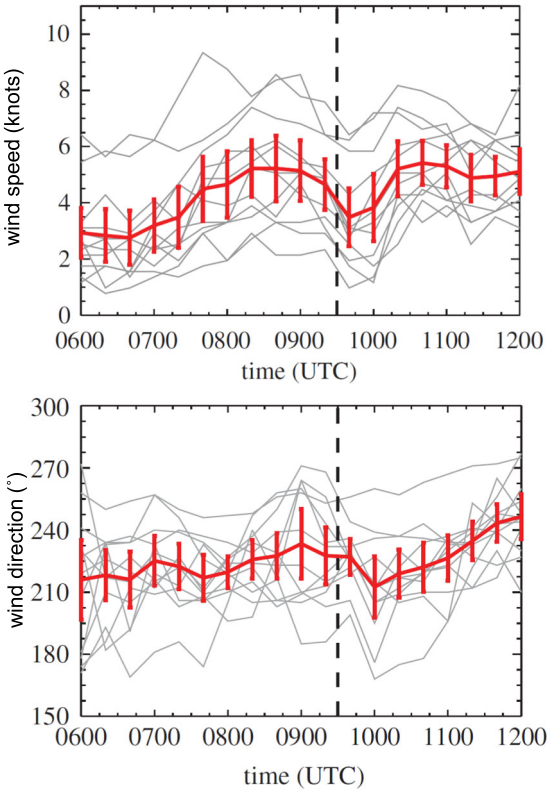


**Fig. 5** Decrease in wind speed approximately 30 min after the strongest obscuration of the sun (upper panel) and the associated change in wind direction (lower panel) during the partial solar eclipse (approx. 90%) on 20 March 2015 using averages (thick line) from several stations (thin lines) in the English Midlands, modified from Gray and Harrison (2016), © Authors

1900 in the south-east of the USA (Fig. 6, but also in the Iberian Peninsula and North Africa). This model representation was further developed by Aplin and Harrison (2003) for the total solar eclipse on 11 August 1999, see also Provod (2010). The authors found a significantly smaller radius with cyclonic flow of only 100 miles around the umbra, followed by another at a radius of 3,000 miles and, in between, anticyclonic flow at a radius of 1,000 miles. Despite local influences, the Aplin and Harrison model was considered a more likely explanation than the original Clayton model by Eugster et al. (2017), during the partial solar eclipse (approx. 70%) in Switzerland on 20 March 2015. More extensive systematic investigations of the 'Eclipse Cyclone', which has a surprisingly large spatial extent, are indicated.

### 3.3 Comparison of Eclipse Changes with Morning and Afternoon Transitions

As described earlier, the usual morning and afternoon transitions are regular phenomena (Lothon et al. 2014; Angevine et al. 2020), involving a change in the entire atmospheric boundary layer structure. These are from a stable layer near the ground and a residual layer above it in the morning to a convective boundary layer and vice versa in the afternoon (Stull 1988). The morning transition begins immediately with radiation-induced warming of the surface, which occurs relatively quickly (within 1–2 h). During the afternoon transition, stabilisation near the ground begins in the afternoon and cooling only slowly sets in during the late evening, in the lowest 100 m (Zelený and Foken 1991). Counter-gradient fluxes can

**Table 3** Decrease in wind speed and change in direction after totality or maximum eclipse according to Schulz et al. (2017)

| Eclipse and location | Wind speed before the eclipse, (with measurement height) | Wind speed reduction | Shift in wind direction | Reference |
|---|---|---|---|---|
| 11 Aug. 1999 Camborne, U.K | 3.0 m $s^{-1}$ (5.8 m) | – 2.0 m $s^{-1}$ | 140° to 130° | Aplin and Harrison (2003) |
| 11 Aug. 1999 Freising, Germany | 2.5 m $s^{-1}$ (6.3 m) | – 1.5 m $s^{-1}$ | | Foken et al. (2001) |
| 11 Aug. 1999 Fülöpháza, Hungary | 2.5 m $s^{-1}$ (3.5 m) | – 1.5 m $s^{-1}$ | | Foken et al. (2001) |
| 11 Aug. 1999 Plittersdorf, Germany | 2.5 m $s^{-1}$ (17 m) | – 1.5 m $s^{-1}$ | | Ahrens et al. (2001) |
| 23 Nov. 2003 Dome Fuji, Antarctica | 6.5 m $s^{-1}$ (10 m) | – 0.3 m $s^{-1}$ | < 5° | Kameda et al. (2009) |
| 29 March 2006 Ibadan, Nigeria | 2.0 m $s^{-1}$ (1 m) | – 1.0 m $s^{-1}$ | | Nymphas et al. (2012) |
| 01 Aug. 2008 Adventdalen, Svalbard (partial) | 4.0 m $s^{-1}$ (3.5 m) | – 2.0 m $s^{-1}$ | | Sjöblom (2010) |
| 20 March 2015 Ny-Ålesund, Svalbard | 2.5 m $s^{-1}$ (2.1 m) | – 1.5 m $s^{-1}$ | 180° to 225° *) | Schulz et al. (2017) |
| 20 March 2015 Midlands, UK (partial) | 5.0 m $s^{-1}$ (4 m) | – 1.5 m $s^{-1}$ | approx. 10° | Gray and Harrison (2016) |
| 08 April 2024 Chazy, NY, USA | 4.0 m $s^{-1}$, 10 m | – 2.5 m $s^{-1}$ | | Wang et al. (2024) |

*The strong rotation of the wind is due to the onset of a katabatic wind from a glacier

arise due to the temperature gradient, which is stable in the lower part and unstable in the upper part (Blay-Carreras et al. 2014). In principle, the morning and afternoon transition approximately corresponds to the conditions after and before totality. However, due to the significantly shorter timescales associated with a solar eclipse, the boundary layer effects in particular have not yet been adequately observed, even though isolated attempts have been made using frequent radiosonde launches (Maturilli and Ritter 2016). With the increased use of remote sensing techniques, e.g. Doppler lidar, progress can be expected here, as has already been shown by Wang et al. (2024).

Complex boundary layer structures also occur in mountain valleys when the mountain-valley wind changes to a valley-mountain wind in the morning. This causes a brief period of calm, during which free convection can occur if there is sufficient solar radiation (Eigenmann et al. 2009). During a solar eclipse the minimum wind speed occurs about half an hour after totality, by which time sufficient radiation has again become available to support convection, hence the transitional effect should also be possible to observe.

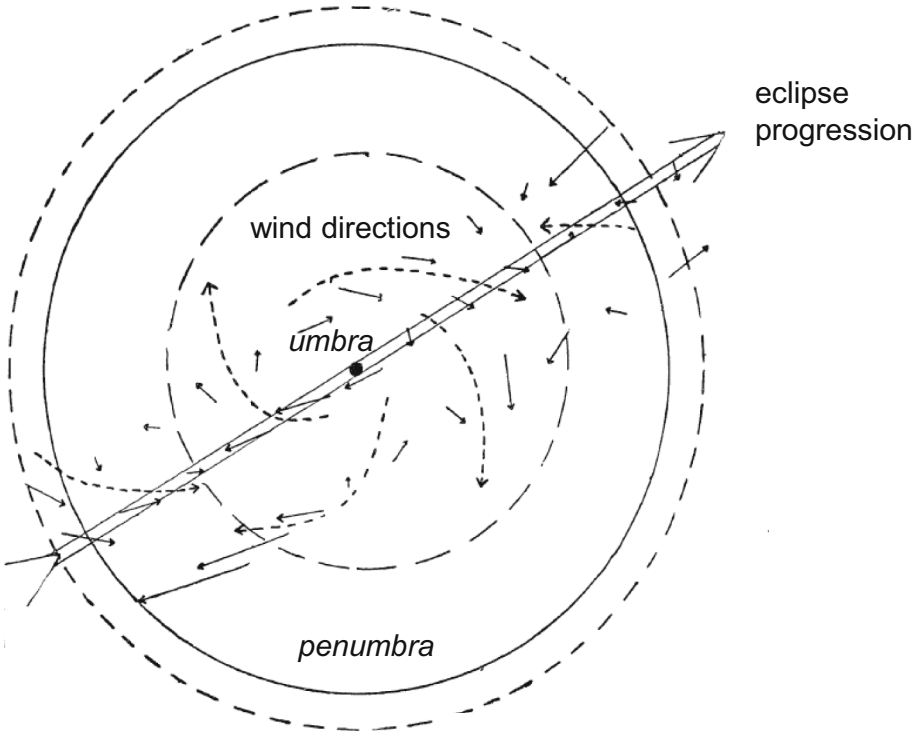


**Fig. 6** Schematic illustration of the 'Eclipse Cyclone' according to Clayton (1901a) based on the total solar eclipse on 28 May 1900 in the USA, © Author

The change in the stratification can be shown using the Obukhov-Lettau stability parameter (Foken and Börngen 2021):

$$\frac{z}{L} = \frac{\kappa z \frac{g}{T} \frac{H}{\rho c_p}}{u_*^3}, \tag{2}$$

in which the quantities are the height $z$, the Obukhov length $L$, the von-Kármán constant $\kappa$, the gravitational acceleration $g$, the air temperature $T$, the sensible heat flux $H$, the air density $\rho$, and the specific heat at constant pressure $c_p$. Figure 7 shows an example of the variation in the stability parameter during an eclipse. About 10–15 min before totality, the stratification becomes stable, $z/L > 0$. At the minimum in the friction velocity, approximately 30 min after totality, there is a sudden change to unstable stratification, whereby the stability parameter assumes values more typical of free convection ($z/L < -1$) due to the combination of reduced friction velocity and substantial increase in the sensible heat flux.

An example of circulation changes in a mountain valley according to Eigenmann et al. (2009) is shown in Fig. 8b, d. As the friction velocity decreases, a positive vertical wind speed develops in the lowest 400 m of the boundary layer, indicating free convection. This effect was corroborated by a large eddy simulation (Brötz et al. 2014). Wang et al. (2024) showed similar behaviour for the total solar eclipse on 8 April 2024. Positive vertical winds in the boundary layer decreased until totality (Fig. 8c). About 30 min after totality, when the wind speed reached its minimum (Fig. 8a), positive vertical winds in the boundary layer became

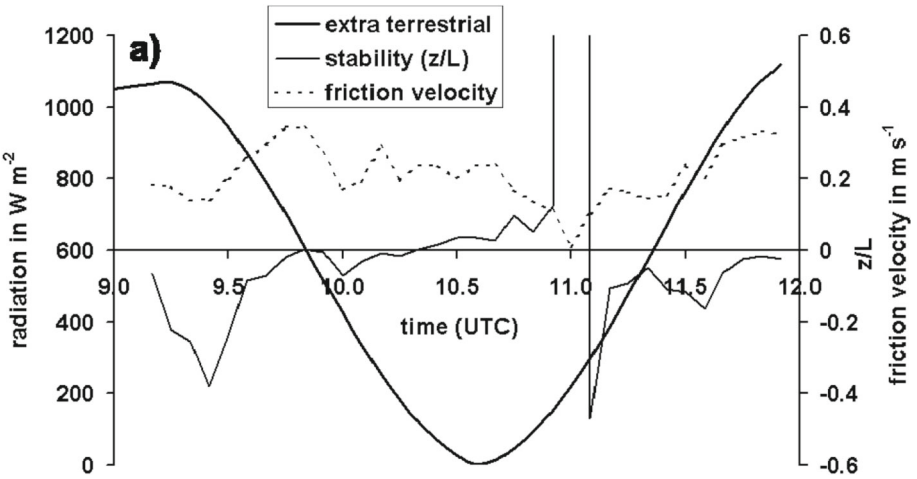


**Fig. 7** Variation of the friction velocity and the stability parameter $z/L$ during the total solar eclipse on 11 August 1999, from Foken et al. (2001), © Authors

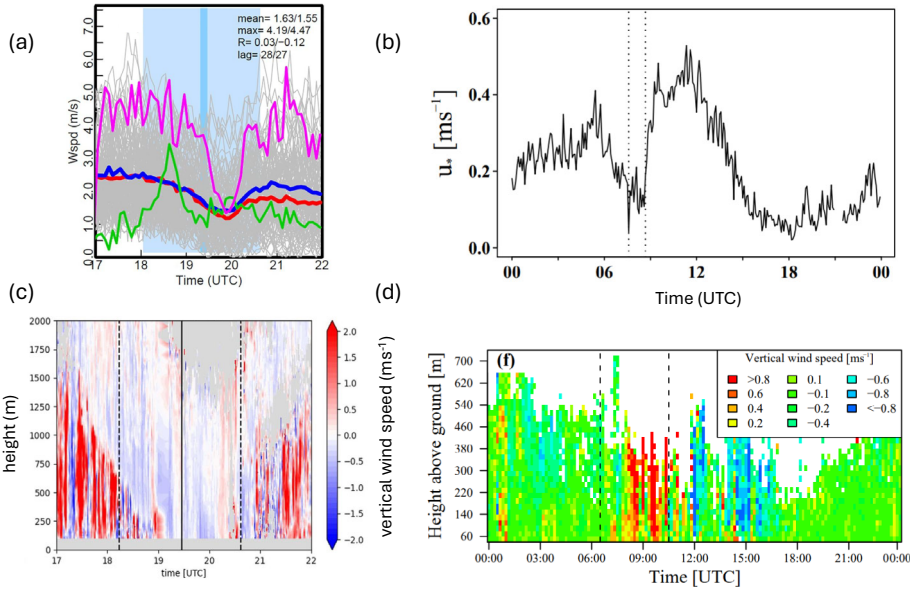


**Fig. 8** Comparison of boundary layer effects during a total solar eclipse, 8 April 2024, Chazy, NY, USA (Wang et al. 2024), (**a**) and (**c**), and during the transition from mountain-valley wind to valley-mountain wind in the morning in the Kinzig Valley (Black Forest, Germany), COPS experiment, Case 8b (**b**) and Case 15a (**d**) after Eigenmann et al. (2009). For better visibility, two different cases were selected in (**b**) and (**d**), whereby the relevant area is dashed. (**a**) shows the wind speed (magenta) and (**b**) the friction velocity and (**c**) vertical wind in the boundary layer measured with Doppler lidar (**d**) and Doppler sodar. ©Authors

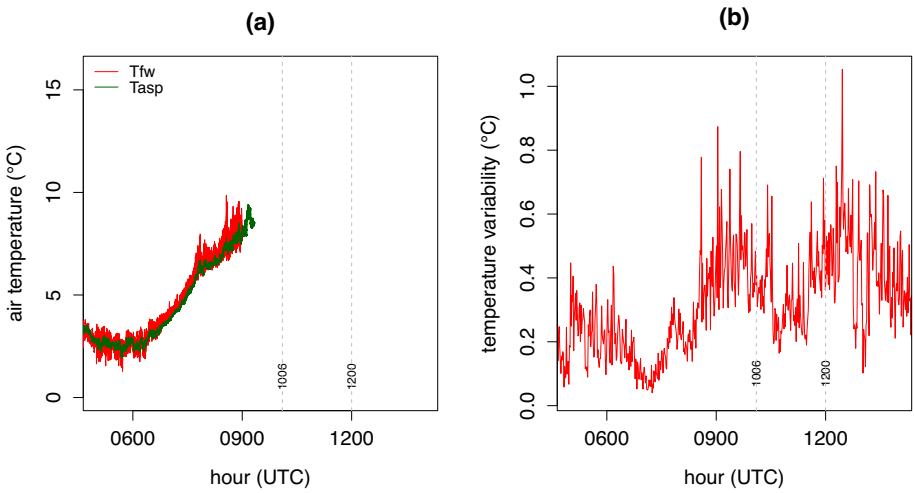


**Fig. 9** (**a**) Time variation of the air temperature measured with a fine wire (Tfw) and aspirated (Tasp) thermometer at 1 s sampling and (**b**) the derived 1- minute standard deviation of the Tfw temperatures during the partial solar eclipse between 1006 and 1200 UTC on 29 March 2025 in Reading, UK, with 31% coverage at 1102 UTC

established relatively quickly due to the existing solar radiation. There is clear similarity between the two cases.

Even during partial solar eclipses, the stability effect is clearly visible, as shown in Fig. 9 for the eclipse on 29 March 2025 with 31% coverage at 1102 UTC in Reading, UK. The eclipse is barely noticeable in the temperature recording (Fig. 9a), but it is visible in the standard deviation of the air temperature (Fig. 9b). The reason for this is the lack of convective cell development, evident in the stability dependence of the so-called integral turbulence characteristics (for an overview, see Foken and Mauder 2024):

$$\frac{\sigma_T}{T_*} = c\left(z/L\right)^{-1/3}, \tag{3}$$

with the standard deviation of the air temperature $\sigma_T$, the dynamic temperature $T_* = -\overline{w'T'}/u_*$, and a constant c $\approx$ 1. Thus, even partial solar eclipses can influence exchange conditions in the atmospheric boundary layer.

## 4 Conclusions

The examples selected demonstrate that total solar eclipses provide an ideal set of circumstances for a natural experiment with rapid onset and cessation of solar radiation. With precisely prescribed radiative changes, processes can be identified and studied that are otherwise difficult to represent or separate from others. These include the time delays between

**Table 4** Upcoming total solar eclipses in the next 10 years. Eclipses with optimal conditions near the solar zenith and regions anticipated to have a sufficient density of measuring instruments are shown in bold

| Date | Terrestrial time | Duration | Area |
|---|---|---|---|
| August 12, 2026 | 17:47:06<br>about 20:30 LT (Spain) | 2:18 | Greenland, Iceland, Spain, Northeastern Portugal |
| August 2, 2027 | 10:07:50<br>about 10:45 LT<br>(Spain) | 6:23 | Morocco, Spain, Algeria, Tunisia, Libya, Egypt, Saudi Arabia, Yemen, Somalia |
| July 22, 2028 | 02:56:40<br>about 13:50 LT (Australia) | 5:10 | Australia, New Zealand |
| November 25, 2030 | 06:51:37<br>about 07:30 LT (South Africa) | 3:44 | Namibia, Botswana, South Africa, Lesotho, Australia |
| March 30, 2033 | 18:02:36<br>about 09:50 LT (Alaska) | 2:37 | Russian Far East, Alaska |
| March 20, 2034 | 10:18:45<br>About 13:00 LT (Egypt) | 4:09 | Nigeria, Cameroon, Chad, Sudan, Egypt, Saudi Arabia, Kuwait, Iran, Afghanistan, Pakistan, India, China (Tibet) |
| September 02, 2035 | 01:56:46<br>About 11:00 LT (Japan) | 2:54 | Northern China, North Korea, Japan |

changes in different variables and fluxes which affect the wind field, extending through to mesoscale processes. Stability-dependent phenomena in particular can be investigated in detail. The application not only improves our understanding of meteorological processes and their parameterisation, but also has an impact on optimising the use of photovoltaics (Harrison and Hanna 2016; Madhavan and Venkat Ratnam 2021) and wind energy, for example.

Given the large number of international measurement programmes applied to atmospheric trace gases, meteorological variables, turbulent fluxes and ecological data (Philipona 2021; Schmid and Rebmann 2021), as well as mesoscale measurement programmes (Brotzge and Fiebrich 2021), high resolution observations are likely to exist in the vicinity of a total solar eclipse region. These observations can underpin the perspective of a natural laboratory experiment without significant additional effort. It is desirable to measure turbulent fluxes with high temporal resolution (eg at 1 min resolution or better), combined with remote sensing technology to determine properties of the lower boundary layer.

To motivate future experiments, Table 4 shows the astronomical data for total solar eclipses over the next 10 years. Unfortunately, the moment of totality can occur at any time—and not always close to solar noon, as would be desirable for the largest changes in meteorological quantities—but the total eclipses in 2027 in Spain and North Africa and in 2028 in Australia and New Zealand, at least, should provide an opportunity to use and exploit this unusual natural laboratory. We encourage as wide a scientific participation in this as possible.

**Acknowledgements** We thank the many previous researchers who have made eclipse measurements which have facilitated this paper's perspective. Technical staff in the Department of Meteorology assisted with the measurements leading to fig 9. The University of Reading supported Open Access publication.

**Authors Contribution** Both authors refined the ideas and contributed equally.

**Data availability** Apart from Fig. 9 (data available at https://doi.org/10.6084/m9.figshare.31333018), no data was collected for this publication. The R program for flux calculation with wavelet analysis was written by Dr. Carsten Schaller (carsten.schaller@uni-muenster.de).

## Declarations

**Conflict of interest** The authors declare no competing interests.



## References

Ahrens D, Iziomon MG, Jaeger L, Matzarakis A, Mayer H (2001) Impacts of the solar eclipse of 11 August 1999 on routinely recorded meteorological and air quality data in south-west Germany. Meteorol Z 10:215–223. https://doi.org/10.1127/0941-2948/2001/0010-0215

Anderson J (1999) Meteorological changes during a solar eclipse. Weather 54:207–251. https://doi.org/10.1002/j.1477-8696.1999.tb06465.x

Angevine WM, Edwards JM, Lothon M, LeMone MA, Osborne SR (2020) Transition periods in the diurnally-varying atmospheric boundary layer over land. Boundary-Layer Meteorol 177(2):205–223. https://doi.org/10.1007/s10546-020-00515-y

Anonymous (1834) Meteorological observations during the solar eclipse of 30th November. 1834, at Boston, Mass. The Boston Medical and Surgical Journal Dec 10, 1834 American Periodicals Series II, Boston

Antonia RA, Chambers AJ, Phong-Anant D, Rajagopalan S, Sreenivasan KR (1979) Response of atmospheric surface layer turbulence to a partial solar eclipse. J Geophys Res Oceans 84(C4):1689–1692. https://doi.org/10.1029/JC084iC04p01689

Aplin KL, Harrison RG (2003) Meteorological effects of the eclipse of 11 August 1999 in cloudy and clear conditions. Proc Roy Soc Lond A Math Phys Eng Sci 459(2030):353–371. https://doi.org/10.1098/rspa.2002.1042

Aplin KL, Scott CJ, Gray SL (2016) Atmospheric changes from solar eclipses. Philos Trans Roy Soc Lond A Phys Eng Sci 374(2077):20150217. https://doi.org/10.1098/rsta.2015.0217

Birt WR (1836) Mr W. R Birt's meteorological observations made during the solar eclipse of May 15, 1836 at Greenwich. Lond Edinb Phil Mag J Sci 9:393–394

Blay-Carreras E, Pardyjak ER, Pino D, Alexander DC, Lohou F, Lothon M (2014) Countergradient heat flux observations during the evening transition period. Atmos Chem Phys 14(17):9077–9085. https://doi.org/10.5194/acp-14-9077-2014

Brötz B, Eigenmann R, Dörnbrack A, Foken T, Wirth V (2014) Early-morning flow transition in a valley in low-mountain terrain. Boundary-Layer Meteorol 152:45–63. https://doi.org/10.1007/s10546-014-9921-7

Brotzge JA, Fiebrich CA (2021) Mesometeorological networks. In: Foken T (ed) Springer handbook of atmospheric measurements. Springer, Cham, pp 1233–1245. https://doi.org/10.1007/978-3-030-52171-4_45

Clayton HH (1901a) The eclipse cyclone and the diurnal cyclones. Ann Astronom Observ Harvard College 41:5–35

Clayton HH (1901b) The eclipse cyclone, the diurnal cyclones, and the cyclones and anticyclones of temperate latitudes. Quart J Roy Meteorol Soc 27(120):269–292. https://doi.org/10.1002/qj.49702712004

Eaton FD, Hines JR, Hatch WH, Cionco RM, Byers J, Garvey D, Miller DR (1997) Solar eclipse effects in the planetary boundary layer over a desert. Boundary-Layer Meteorol 83:331–346. https://doi.org/10.1023/A:1000219210055

Economou G, Christou ED, Giannakourou A, Gerasopoulos E, Georgopoulos D, Kotoulas V, Lyra D, Tsakalis N, Tzortziou M, Vahamidis P, Papathanassiou E, Karamanos A (2008) Eclipse effects on field crops and

marine zooplankton: the 29 March 2006 total solar eclipse. Atmos Chem Phys 8(16):4665–4676. https://doi.org/10.5194/acp-8-4665-2008
Eigenmann R, Metzger S, Foken T (2009) Generation of free convection due to changes of the local circulation system. Atmos Chem Phys 9:8587–8600. https://doi.org/10.5194/acp-9-8587-2009
Elmhamdi A, Roman MT, Peñaloza-Murillo MA, Pasachoff JM, Liu Y, Al-Mostafa ZA, Maghrabi AH, Oloketuyi J, Al-Trabulsy HA (2024) Impact of the eclipsed sun on terrestrial atmospheric parameters in desert locations: a comprehensive overview and two events case study in Saudi Arabia. Atmosphere 15(1):62. https://doi.org/10.3390/atmos15010062
Eugster W, Emmel C, Wolf S, Buchmann N, McFadden JP, Whiteman CD (2017) Effects of vernal equinox solar eclipse on temperature and wind direction in Switzerland. Atmos Chem Phys 17(24):14887–14904. https://doi.org/10.5194/acp-17-14887-2017
Foken T (2021) Springer handbook of atmospheric measurements. Springer, Cham. https://doi.org/10.1007/978-3-030-52171-4
Foken T, Bange J (2021) Temperature sensors. In: Foken T (ed) Springer handbook of atmospheric measurements. Springer, Cham, pp 183–208. https://doi.org/10.1007/978-3-030-52171-4_7
Foken T, Börngen M (2021) Lettau's contribution to the Obukhov length scale: a scientific historical study. Boundary-Layer Meteorol 179:369–383. https://doi.org/10.1007/s10546-021-00606-4
Foken T, Mauder M (2024) Micrometeorology, 3 Ed. Springer, Cham. https://doi.org/10.1007/978-3-031-47526-9
Foken T, Wichura B, Klemm O, Gerchau J, Winterhalter M, Weidinger T (2001) Micrometeorological conditions during the total solar eclipse of August 11 1999. Meteorol Z 10:171–178. https://doi.org/10.1127/0941-2948/2001/0010-0171
Foken T, Leuning R, Oncley SP, Mauder M, Aubinet M (2012) Corrections and data quality. In: Aubinet M, Vesala T, Papale D (eds) Eddy covariance: a practical guide to measurement and data analysis. Springer, Dordrecht, pp 85–131. https://doi.org/10.1007/978-94-007-2351-1_4
Foken T, Kartschall T, Badeck F, Waloszczyk K, Wichura B, Gerchau J (2000) Time response characteristics for the atmosphere-plant-interaction, measured during the total solar eclipses in Southern Germany on August 11, 1999. In: 14th Symposium on Boundary Layer and Turbulence, 7–11 Aug. 2000 2000. Am. Meteorol. Soc., Boston, pp 159–160
Founda D, Melas D, Lykoudis S, Lisaridis I, Gerasopolous E, Kouvarakis G, Petrakis M, Zerefos C (2007) The effect of the total solar eclipse of 29 March 2006 on meteorological variables in Greece. Atmos Chem Phys 7:5543–5553. https://doi.org/10.5194/acp-7-5543-2007
Fowler J, Wang J, Ross D, Colligan T, Godfrey J (2019) Measuring ARTSE2017: results from Wyoming and New York. Bull Am Meteorol Soc 100(6):1049–1060. https://doi.org/10.1175/BAMS-D-17-0331.1
Garreaud R, Bozkurt D, Spangrude C, Carrasco-Escaff T, Rondanelli R, Muñoz R, Jubier XM, Lazzara M, Keller L, Rojo P (2023) Cooling the coldest continent: the 4 December 2021 total solar eclipse over Antarctica. Bull Am Meteorol Soc 104(12):E2265–E2285. https://doi.org/10.1175/BAMS-D-22-0272.1
Gray SL, Harrison RG (2016) Eclipse-induced wind changes over the British Isles on the 20 March 2015. Philos Trans Roy Soc Lond A Math Phys Eng Sci 374:20150224. https://doi.org/10.1098/rsta.2015.0224
Harrison G, Gray S (2017) The weather's response to a solar eclipse. Astron Geophys 58:4.11–14.16. https://doi.org/10.1093/astrogeo/atx135
Harrison RG, Hanna E (2016) The solar eclipse: a natural meteorological experiment. Philos Philos Trans Roy Soc Lond A Phys Eng Sci 374:20150225. https://doi.org/10.1098/rsta.2015.0225
Hicks BB, Pendergrass WR, Oetting JN, O'Dell DL, Eash NS (2021) The North American Solar Eclipse of 2017: observations on the surface biosphere, time responses and persistence. Boundary-Layer Meteorol 179(1):1–17. https://doi.org/10.1007/s10546-020-00582-1
Higgins CW, Drake SA, Kelley J, Oldroyd HJ, Jensen DD, Wharton S (2019) Ensemble-averaging resolves rapid atmospheric response to the 2017 total solar eclipse. Front Earth Sci 7:198. https://doi.org/10.3389/feart.2019.00198
Hudgins L, Friehe CA, Mayer ME (1993) Wavelet transforms and atmopsheric turbulence. Phys Rev Lett 71(20):3279–3282. https://doi.org/10.1103/PhysRevLett.71.3279
Jenki S, Makra L, Sodár I, Horváth S, Domonkos P (1999) Solar eclipse, Legkor, vol XLIV, pp 6–20 (**in Hungarian**)
Jenyns L (1858) Observations in meteorology: relating to temperature, the winds, atmospheric pressure, the aqueous phenomena of the atmosphere, weather-changes, etc. J. Van Voorst, London. https://doi.org/10.5962/bhl.title.133874
Kameda T, Fujita K, Sugita O, Hirasawa N (2009) Total solar eclipse over Antarctica on 23 November 2003 and its effects on the atmosphere and snow near the ice sheet surface at Dome Fuji. J Geophys Res 114:D18115. https://doi.org/10.1029/2009JD011886

Kapoor RK, Adiga BB, Singal SP, Aggarwal SK, Gera BS (1982) Studies of the atmospheric stability characteristics during the solar eclipse of February 16, 1980. Boundary-Layer Meteorol 24:415–419. https://doi.org/10.1007/BF00120730

Lazzus JA, Vega-Jorquera P, Pacheco R, Luis Tamblay L, Martínez-Ledesma M, Ovalle EM, Carrasco E, Bravo M, Villalobos CU, Salfate I, Palma-Chilla L, Foppiano AJ (2022) Changes in meteorological parameters during the total solar eclipse of 2 July 2019 in La Serena, Chile. Ann Geophys 65:PA531. https://doi.org/10.4401/ag-8623

Leeds-Harrison P, Youngs EG, Blackburn DWK (2002) Soil temperatures during the solar eclipse on 11 August 1999. Eur J Soil Sci 51:183–184. https://doi.org/10.1046/j.1365-2389.2000.00293.x

Lothon M, Lohou F, Pino D, Couvreux F, Pardyjak ER, Reuder J, de Vilà-Guerau Arellano J, Durand P, Hartogensis O, Legain D, Augustin P, Gioli B, Lenschow DH, Faloona I, Yagüe C, Alexander DC, Angevine WM, Bargain E, Barrié J, Bazile E, Bezombes Y, Blay-Carreras E, van de Boer A, Boichard JL, Bourdon A, Butet A, Campistron B, de Coster O, Cuxart J, Dabas A, Darbieu C, Deboudt K, Delbarre H, Derrien S, Flament P, Fourmentin M, Garai A, Gibert F, Graf A, Groebner J, Guichard F, Jiménez MA, Jonassen M, van den Kroonenberg A, Magliulo V, Martin S, Martinez D, Mastrorillo L, Moene AF, Molinos F, Moulin E, Pietersen HP, Piguet B, Pique E, Román-Cascón C, Rufin-Soler C, Saïd F, Sastre-Marugán M, Seity Y, Steeneveld GJ, Toscano P, Traullé O, Tzanos D, Wacker S, Wildmann N, Zaldei A (2014) The BLLAST field experiment: boundary-layer late afternoon and sunset turbulence. Atmos Chem Phys 14(20):10931–10960. https://doi.org/10.5194/acp-14-10931-2014

Madhavan BL, Venkat Ratnam M (2021) Impact of a solar eclipse on surface radiation and photovoltaic energy. Sol Energy 223:351–366. https://doi.org/10.1016/j.solener.2021.05.062

Maturilli M, Ritter C (2016) Surface radiation during the total solar eclipse over Ny-Ålesund, Svalbard, on 20 March 2015. Earth Syst Sci Data 8(1):159–164. https://doi.org/10.5194/essd-8-159-2016

Mauder M, Desjardins RL, Oncley SP, MacPherson JI (2007) Atmospheric response to a solar eclipse over a cotton field in Central California. J Appl Meteorol Climatol 46:1792–1803. https://doi.org/10.1175/2007JAMC1495.1

Mauder M, Foken T, Aubinet M, Ibrom A (2021) Eddy-covariance measurements. In: Foken T (ed) Springer handbook of atmospheric measurements. Springer, Cham, pp 1473–1504. https://doi.org/10.1007/978-3-030-52171-4_55

Nymphas EF, Otunla TA, Adeniyi MO, Oladiran EO (2012) Impact of the total solar eclipse of 29 March 2006 on the surface energy fluxes at Ibadan, Nigeria. J Atmos Sol-Terr Phys 80:28–36. https://doi.org/10.1016/j.jastp.2012.02.024

Peñazola-Murillo MA (2002) Optical response of the atmospheric during Caribbean total solar eclipses of the 26 February 1998 and on 3 February of 1916 at Falcon state, Venezuela. Earth Moon Planets 91:125–159. https://doi.org/10.1023/A:1022417600232

Percival DB, Walden AT (2000) Wavelet methods for time series analysis. Cambridge University Press, Cambridge. https://doi.org/10.1017/CBO9780511841040

Philipona R (2021) Networks of atmospheric measuring techniques. In: Foken T (ed) Springer handbook of atmospheric measurements. Springer, Cham, pp 1687–1712. https://doi.org/10.1007/978-3-030-52171-4_63

Provod M (2010) Solar eclipse-induced lower atmosphere changes. The University of Reading, Reading

Satyaningsih R, Heriyanto E, Kadarsah NTA, Rizal J, Sopaheluwakan A, Aldrian E (2016) Impacts of the total solar eclipse of 9 March 2016 on meteorological parameters in Ternate. J Phys Conf Ser 771:012014. https://doi.org/10.1088/1742-6596/771/1/012014

Schaller C, Göckede M, Foken T (2017) Flux calculation of short turbulent events—comparison of three methods. Atmos Meas Tech 10:869–880. https://doi.org/10.5194/amt-10-869-2017

Schmid HP, Rebmann C (2021) Integration of meteorological and ecological measurements. In: Foken T (ed) Springer handbook of atmospheric measurements. Springer, Cham, pp 1713–1725. https://doi.org/10.1007/978-3-030-52171-4_64

Schulz A, Schaller C, Maturilli M, Boike J, Ritter C, Foken T (2017) Surface energy fluxes during the total solar eclipse over Ny-Ålesund, Svalbard, on 20 March 2015. Meteorol Z 26(4):431–440. https://doi.org/10.1127/metz/2017/0846

Sjöblom A (2010) A solar eclipse seen from the High Arctic during the period of midnight sun: effects on the local meteorology. Meteorol Atmos Phys 107(3):123–136. https://doi.org/10.1007/s00703-010-0070-3

Stull RB (1988) An introduction to boundary layer meteorology. Kluwer, Dordrecht. https://doi.org/10.1007/978-94-009-3027-8

Torrence C, Compo GP (1998) A practical guide to wavelet analysis. Bull Am Meteorol Soc 79:61–78. https://doi.org/10.1175/1520-0477(1998)079%3c0061:APGTWA%3e2.0.CO;2

Wang J, Dai A, Yu C-L, Shrestha B, McGuinnes DJ, Bain N (2024) Characterizing the impacts of 2024 total solar eclipse using New York State Mesonet data. Geophys Res Lett 51:e2024GL112684. https://doi.org/10.1029/2024GL112684

Zelený J, Foken T (1991) Ausgewählte Ergebnisse des Grenzschichtexperimentes in Bohunice 1989. Z Meteorol 41:439–445